

Characterization of guided resonances in photonic crystal slabs using terahertz time-domain spectroscopy

Zhongping Jian and Daniel M. Mittleman^{a)}

Department of Electrical and Computer Engineering, Rice University, MS-366, P.O. Box 1892, Houston, Texas 77251-1892

(Received 14 August 2006; accepted 25 September 2006; published online 29 December 2006)

We describe experimental studies of guided resonances in two-dimensional photonic crystal slabs using coherent single-cycle terahertz pulses. Our measurements directly reveal two stages of pulse transmission in the time domain: an initial pulse resulting from the direct transmission through the photonic crystal slab and a long-lived decaying tail resulting from the finite lifetime of guided resonance modes. These reflect the coupling of a set of discrete modes to the free-space continuum, which produces guided resonances with Fano resonance profiles. Phase spectra are also obtained experimentally, and these also exhibit the signatures of guided resonances. By changing the incident angle of the input beam, we change the spectrum of guided resonances excited by the incident wave. Our experimental results are in good agreement with numerical simulations. © 2006 American Institute of Physics. [DOI: 10.1063/1.2399335]

INTRODUCTION

Photonic crystals are materials that exhibit periodicity in the dielectric function in one or more dimensions.^{1–3} They have been intensively investigated both theoretically and experimentally because of their promise of manipulating the flow of electromagnetic radiation. Although a three-dimensional photonic crystal is desired to completely confine the radiation fields, it is difficult to fabricate such structures. Much attention, therefore, has been directed towards two-dimensional photonic crystals of finite thickness, which are generally referred to as photonic crystal slabs.⁴

In a photonic crystal slab, light is confined within the plane of the slab by a two-dimensional periodic dielectric structure, and in the third dimension by total internal reflection resulting from the refractive index contrast between the slab and the cladding. Because of the internal reflection condition, this confinement in the third dimension is not complete. Some modes are guided, while others can couple to external radiation modes. These latter modes, with finite lifetimes inside the slab, have been described as leaky modes or more recently as guided resonances.^{5–9} Since these discrete resonances couple to a continuum of free-space modes, they exhibit a Fano resonance line shape.⁹ In a band structure, confined modes and guided resonances are separated by the light line: the modes that cannot couple to external radiation are below the light line, while the guided resonances that have finite lifetime due to coupling to external propagating modes are above the light line.⁴ This coupling provides a way to excite these guided resonances using external waves. However, it has also been noted that some modes above the light line are also not leaky, but trapped inside the slab, because the coupling between them and external modes is prohibited by the mismatching of spatial symmetries.^{10–12} This provides the possibility of a complete confinement of certain

guided resonance modes by photonic crystal slabs, although the method by which such modes could be efficiently excited remains unclear.

In spite of their importance, the study of guided resonances has lagged behind the more common studies of the guided modes which are confined in the plane of the slab. In particular, there have been very few experimental reports on the temporal behavior of guided resonances. Of the few experimental studies of guided resonances, almost all have focused on their power transmission spectra, and not on their phase response.^{7,11–17} Here we report the investigation of guided resonances using terahertz time-domain spectroscopy.¹⁸ This technique involves the generation and detection of single-cycle pulses of terahertz radiation, with a broad bandwidth in the far infrared ($\lambda=200\text{--}6000\ \mu\text{m}$). The coherent detection of the transmitted electric field in the time domain with subcycle temporal resolution permits the direct measurement of the amplitude and phase spectrum of a sample.^{19–23}

EXPERIMENTAL RESULTS

To excite guided resonances, we employ an out-of-plane illumination scheme, as shown in Fig. 1. Because of the long wavelength of the radiation source, the spatial periodicity of the dielectric function is in the range of hundreds of microns. As a result, essentially perfect crystals can be fabricated using conventional etching. Defects and interface roughness effects are almost negligible. For this study, our photonic crystal slab consists of a $300\ \mu\text{m}$ -thick high-resistivity ($\rho > 10^4\ \Omega\ \text{cm}$) silicon wafer with holes etched all the way through, using deep reactive ion etching.²⁴ The holes have diameters of $360\ \mu\text{m}$, and they are arranged on a $400\ \mu\text{m}$ hexagonal lattice. High-resistivity silicon is an ideal material for such studies because of its low absorption and frequency-independent refractive index in the relevant spectral range.²⁵ Terahertz pulses are generated using photoconducting antennas.²⁶ Linearly polarized terahertz pulses are collimated

^{a)}Fax: (713) 348-5686; electronic mail: daniel@rice.edu

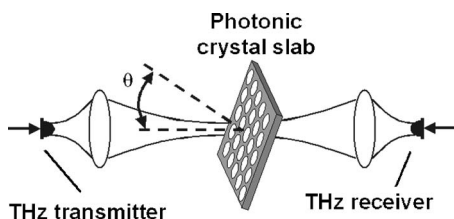


FIG. 1. A schematic of the experimental setup to excite the guided resonances in photonic crystal slabs. p -polarized terahertz pulses are incident at angle θ relative to the surface normal of the slab. The transmitted waves are detected on the other side of the slab. For all of the data shown in this paper, the in-plane component of the wave vector of the incident wave is along the Γ - K direction of the hexagonal photonic crystal lattice. The photonic crystal slab is made of high-resistivity silicon and its thickness is $300\ \mu\text{m}$. The air holes have diameters of $360\ \mu\text{m}$ and they are arranged on a hexagonal lattice with a pitch of $400\ \mu\text{m}$.

by a polyethylene lens and then transmitted through the sample. The terahertz spot size is much larger than the lattice constant of the photonic crystal slab, so many holes are illuminated. A second polyethylene lens images the transmitted terahertz waves onto a photoconductive receiver, oriented to detect the same polarization. For comparison, we have also measured the transmission through an unetched silicon wafer of the same thickness. A reference measurement is also taken when there is no sample present, which we refer to as an air signal.

As a first demonstration, we study the samples at normal incidence, that is, at an incident angle $\theta=0^\circ$. In these measurements, the input polarization is oriented along the Γ - K axis of the hexagonal lattice, although identical results are obtained for Γ - M polarization as well. Figure 2 shows typical measured wave forms. The reference signal (air) is a single-cycle pulse of ~ 1 ps duration, with a broad bandwidth spanning from 0.05 to 1.5 THz. The solid silicon wafer shows pronounced recurrences in the time domain due to multiple reflections in the slab. These recurrences are also present in the wave form transmitted through the photonic crystal slab, but in this case, there are additional pronounced

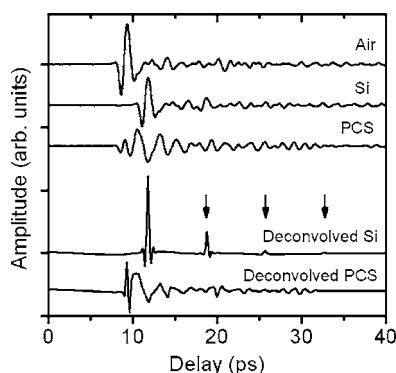


FIG. 2. Typical measured time-domain wave forms after propagating through air, a silicon slab, and the photonic crystal slab (PCS), as labeled. The bottom two curves illustrate the deconvolution of the system response (using the air signal as a reference) from the silicon and photonic crystal wave forms, respectively, using a hybrid Fourier-wavelet based denoising and deconvolution technique (Ref. 27). Fabry-Pérot effect can be clearly observed in the deconvolved silicon wave form, as demonstrated by the multiple reflections noted by the arrows. Two stages of guided resonances can be seen in the deconvolved photonic crystal wave form: an initial pulse followed by a long decaying tail. Wave forms are offset for clarity.

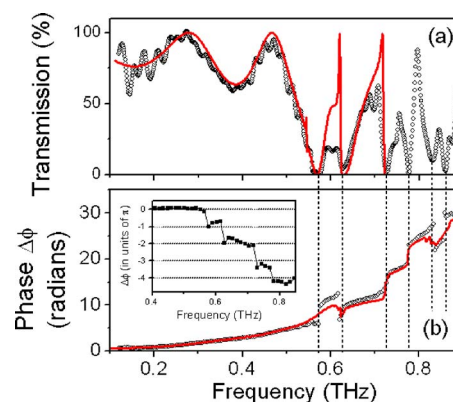


FIG. 3. (Color online) (a) Power transmission spectrum, $|E_S(\omega)/E_R(\omega)|^2$ and (b) relative phase spectrum $\Delta\phi = \phi_S - \phi_R$, where subscript S represents the measured signal after transmitting through the photonic crystal slab and R is the reference air signal. Guided resonances are manifested in the transmission curve by minima in the power spectrum. These are echoed at the same frequencies by abrupt jumps in the phase curve, as shown by the dashed vertical lines. The circles are experiment results. The solid curves in (a) and (b) are finite element method (FEM) and finite-difference time-domain (FDTD) simulation results, respectively. (Inset) We fit a smoothly increasing quartic function to $\Delta\phi$ over the range from 0.15 to 0.85 THz, and then subtract this function from the experimental data. The result shows that the phase of the transmitted radiation changes by π across each resonance.

decaying oscillations, persisting for tens of picoseconds. To distinguish these decaying oscillatory features from the intrinsic system response of the terahertz spectrometer, we employ a hybrid Fourier and wavelet-based scheme to simultaneously denoise and deconvolve the air reference signal from the sample signals.²⁷

The deconvolved results are shown as the bottom two curves in Fig. 2, with both being shifted the same value along the time axis for a better comparison. For the data obtained with the solid silicon slab, three reflected pulses can be clearly observed, as denoted by arrows. These are the manifestations of the Fabry-Pérot effect in the time domain. In contrast, when the incident pulse transmits through the photonic crystal slab, two distinct stages are observed: a broadband initial pulse and a subsequent decaying tail. The initial part comes from the incident waves that transmit directly through the slab. The decaying tail comes from the part of the incident waves that excite guided resonances. Since guided resonances are modes that are not confined inside the photonic crystal slab, they decay out of the slab with various lifetimes. This phenomenon has not been observed experimentally in the time domain, although it has been studied previously by Fan *et al.* using finite-difference time-domain (FDTD) simulations.⁸

The effects of the guided resonances are also clear in the frequency domain. The results are shown in Fig. 3. Here, the power attenuation and phase spectra of the photonic crystal have been obtained by normalization to those of the reference air wave form. We focus specifically on the region where the wavelength of the light is comparable to or larger than the lattice constant of the photonic crystal. At low frequencies (below 0.5 THz), the transmission spectrum of the photonic crystal slab exhibits oscillations similar to Fabry-Pérot oscillations. At frequencies higher than 0.5 THz, numerous transmission minima can be observed. Those minima

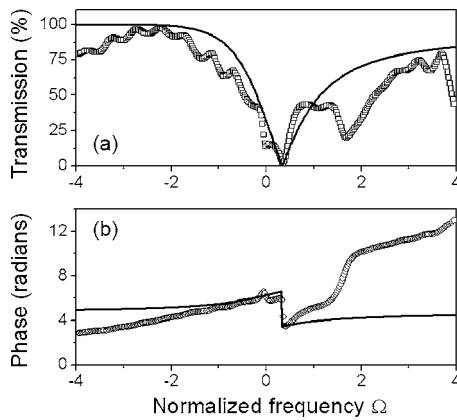


FIG. 4. A close-up view of (a) the amplitude transmission spectrum and (b) the phase difference spectrum shown in Fig. 3, zooming in on the first two guided resonances at ~ 0.56 and ~ 0.63 THz. These data are plotted against a normalized frequency parameter $\Omega = (\nu - \nu_0)/\gamma$, where $\nu_0 = 0.56$ THz and $\gamma = 40$ GHz. The solid lines in (a) and (b) are the amplitude and phase of the Fano line shape, computed using Eq. (1). The higher resonance (at $\Omega \sim 1.8$) is not included in the calculated profile.

are manifestations of guided resonances, with the widths of the minima related to the lifetimes of the resonance modes. We use a finite element method (FEM) simulation to numerically calculate the transmission spectrum. In the calculation, the slab is assumed to be composed of a lossless dielectric with refractive index equal to that of silicon, $n = 3.418$.²⁵ The slab is embedded in vacuum, $n = 1$. The calculated result is shown as the solid curve in Fig. 3(a). As can be seen, it matches very well with the experimental results up to a frequency of 0.72 THz, beyond which we reach the limit of our computational power.

The guided resonances produce interesting features in the phase spectrum as well. We extract the spectral phase from the Fourier transforms of the measured electric fields. The net phase difference $\Delta\varphi(\omega)$ between the signal transmitted through the photonic crystal slab and the air reference is shown in Fig. 3(b). We observe an overall increasing trend in $\Delta\varphi(\omega)$ with increasing frequency, due to the increasingly dispersive behavior of the periodic structure.²¹ Superimposed on this smooth increase, we find several abrupt phase jumps at specific frequencies, which correspond to the frequencies of the transmission minima seen in the transmission spectrum (see dashed vertical lines in Fig. 3). We can fit a smoothly increasing function to this phase variation, and subtract it from the data in order to determine the size of the phase jumps. The result is shown in the inset to Fig. 3(b). As expected for a typical resonance, the phase jumps are all approximately equal to π . The solid line is the result of a FDTD simulation, which can provide phase information and which matches well with the observed phase spectrum.

To show that the guided resonances exhibit the expected Fano line shape, we examine in detail the lowest frequency resonance, at ~ 0.56 THz. In Fig. 4, we plot the measured amplitude transmission and phase difference in the vicinity of this resonance as a function of the normalized frequency parameter $\Omega = (\nu - \nu_0)/\gamma$, where $\nu_0 = 560$ GHz and $\gamma = 40$ GHz. As discussed by Fan *et al.*,⁹ the Fano transmission line shape can be written as

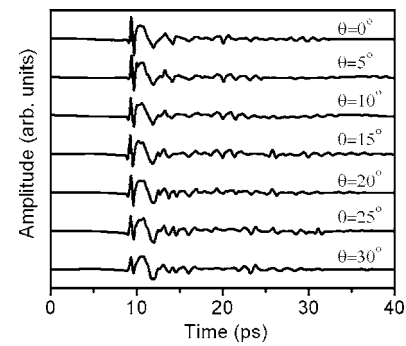


FIG. 5. Deconvolved wave forms for transmission at different incident angles, ranging from 0° to 30° , as labeled. The deconvolution procedure was the same as used to generate the lower two curves in Fig. 2. All of these wave forms have similar structures: an initial broadband pulse followed by a long decaying tail. Differences can be observed, resulting from the excitation of a different set of guided resonances at different angles of incidence. Curves are offset for clarity.

$$t(\Omega) = i\tau + \frac{\rho - i\tau}{1 + i\Omega}, \quad (1)$$

where $\rho = (\bar{n} - 1)/(\bar{n} + 1)$ is the amplitude reflection coefficient, computed using the volume-weighted average refractive index $\bar{n} \approx 1.944$, and where $\tau^2 = 1 - \rho^2$. The solid lines in Fig. 4 show the amplitude and phase of $t(\Omega)$, computed using Eq. (1). The second resonance, at ~ 0.63 THz, also falls within the spectral window displayed in Fig. 4, but the calculated curve only accounts for a single resonance. Also, no attempt has been made to correct the phase data for the smoothly increasing background which is evident in Fig. 3(b), or for the Fabry-Pérot-like oscillations at low frequencies. Even so, there is reasonable correspondence between the experimental and predicted line shapes.

We have also experimentally studied the effects of the angle of incidence on the measured spectra. Changing this angle can lead to the excitation of other guided resonances and can also cause the spectral location of the resonances to shift to either higher or lower frequency. Figure 5 shows deconvolved signals for typical transmitted time-domain wave forms measured at increasing values of θ , using the same deconvolution scheme described above. These results are obtained for *p*-polarized input radiation. As in the case of normal incidence ($\theta = 0^\circ$), all these wave forms are significantly dispersed and all have similar structures: an initial fast pulse and a long decaying tail. Qualitatively, therefore, the results are equivalent to the normal incidence case. We observe that the amplitude of the initial pulse decreases with the incidence angle, which may result from an increasing Fresnel reflectivity of the slab as the angle increases.

Figure 6 shows the power spectra for different incident angles, focusing specifically on the region below 0.75 THz. With the change of the incident angle, additional transmission minima emerge, such as, for example, the pronounced resonance that appears at a frequency slightly above 0.5 THz, and another more subtle feature close to 0.7 THz. These newly emerging guided resonances are excited as a result of the nonzero parallel component of the wave vector. From the angular variation of the spectral positions of the transmission minima, we can extract a band structure for the

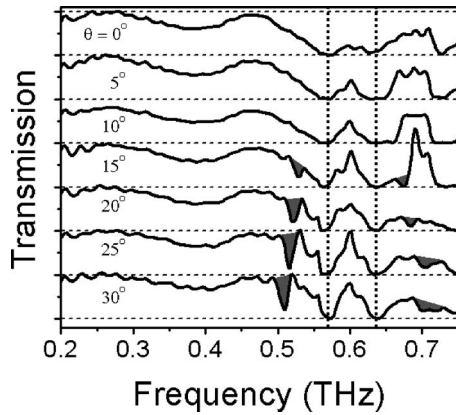


FIG. 6. Power transmission spectra for wave forms measured at different incident angles. As the angle of incidence increases, the nonzero value of the parallel wave vector can lead to the excitation of different guided resonances. In particular, two additional resonances can be seen appearing and shifting with increasing angle, at ~ 0.53 and ~ 0.7 THz (highlighted). In other cases, the resonances exhibit little or no shift as θ increases (see, for example, the two resonances marked by vertical dashed lines). Curves are offset for clarity.

observed guided resonances. This is shown in Fig. 7. Of course, not all modes can efficiently couple to an incident plane wave. This band structure only shows modes which couple to the external incident field, so it is, by necessity, incomplete. Nevertheless, it illustrates modes that shift to higher and lower frequencies with increasing in-plane wave vector k_{\parallel} , as well as several modes that do not shift at all within the accuracy of the measurement. This plurality of behaviors can be qualitatively understood, even in the limit that the air hole diameter shrinks to zero, that is, in the empty lattice approximation. In this case, the dispersion is merely a result of the folding of the in-plane Brillouin zone, which can lead to either positive or negative values of $d\omega/dk_{\parallel}$. This result has recently been discussed in detail by Crozier *et al.*¹⁷

All of the features observed in the transmission curves have their corresponding signatures in the phase spectrum. Figure 8 shows the net phase difference $\Delta\phi(\omega)$ between sample signals and the corresponding reference air signal, for

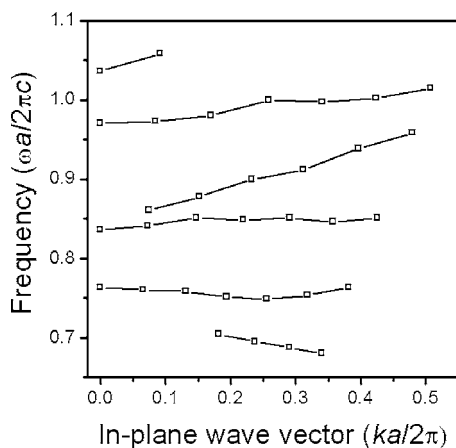


FIG. 7. Spectral positions of the various transmission minima as a function of the angle of incidence, which determines the in-plane wave vector. This band structure illustrates guided resonance modes which shift to higher and lower frequencies with increasing in-plane wave vector, as well as modes which do not shift at all, within the accuracy of the measurements.

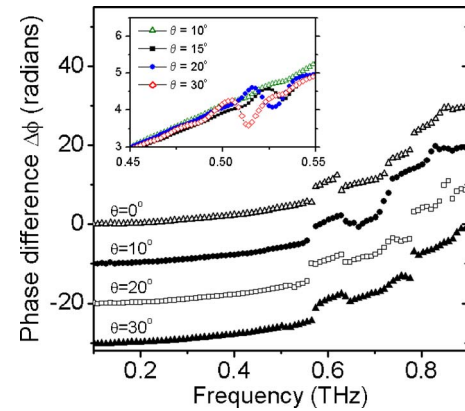


FIG. 8. (Color online) Phase difference spectra [as in Fig. 3(b)] for different incident angles, as labeled in the figure. Curves are offset for clarity. The inset shows an expanded view of the phase spectrum between 0.45 and 0.55 THz for several values of θ . This highlights the feature corresponding to the new guided resonance which is excited in this spectral range at angles $\theta > 10^\circ$.

various values of θ . These curves are very similar, exhibiting the same dispersive effects at frequency below 0.5 THz and guided resonances between 0.5 and 0.9 THz. Subtle differences do exist, however, corresponding to the variations in the transmission spectrum. Shown in the inset is a small portion of the data from Fig. 8. This shows that the guided resonance emerging at 0.53 THz gives rise to a growing feature in the phase spectrum.

CONCLUSION

To conclude, we have experimentally characterized guided resonances in photonic crystal slabs using terahertz time-domain spectroscopy. These resonances give rise to pronounced features in the transmission spectrum of the slab, in both amplitude and phase. We directly observe the two stages in the time domain and jumps in the phase curve, both of which result from the excitation of guided resonances. Further, the excited resonances change as the angle of incidence is varied, a result of the symmetry properties of the various guided resonance modes. Our experimental results are in good agreement with numerical simulation results. These results also highlight the value of pulsed terahertz techniques in studies of guided resonances in photonic crystal slabs, since they permit a complete characterization of these phenomena.

ACKNOWLEDGMENT

This work has been supported in part by the National Science Foundation.

- ¹E. Yablonovitch, Phys. Rev. Lett. **58**, 2059 (1987).
- ²S. John, Phys. Rev. Lett. **58**, 2486 (1987).
- ³J. D. Joannopoulos, R. D. Meade, and J. N. Winn, *Photonic Crystals: Molding the Flow of Light* (Princeton University Press, Princeton, 1995).
- ⁴S. G. Johnson, S. Fan, P. R. Villeneuve, J. D. Joannopoulos, and L. A. Kolodziejski, Phys. Rev. B **60**, 5751 (1999).
- ⁵S. Peng and G. M. Morris, J. Opt. Soc. Am. A **13**, 993 (1996).
- ⁶A. R. Cowan, P. Paddon, V. Pacradouni, and J. F. Young, J. Opt. Soc. Am. A **18**, 1160 (2001).
- ⁷M. C. Netti, A. Harris, J. J. Baumberg, D. M. Whittaker, M. B. D. Charlton, M. E. Zoorob, and G. J. Parker, Phys. Rev. Lett. **86**, 1526 (2001).

- ⁸S. Fan and J. D. Joannopoulos, Phys. Rev. B **65**, 235112 (2002).
- ⁹S. Fan, W. Suh, and J. D. Joannopoulos, J. Opt. Soc. Am. A **20**, 569 (2003).
- ¹⁰P. Paddon and J. F. Young, Phys. Rev. B **61**, 2090 (2000).
- ¹¹V. Pacradouni, W. J. Mandeville, A. R. Cowan, P. Paddon, J. F. Young, and S. R. Johnson, Phys. Rev. B **62**, 4204 (2000).
- ¹²T. Ochiai and K. Sakoda, Phys. Rev. B **63**, 125107 (2001).
- ¹³M. Kanskar, P. Paddon, V. Pacradouni, R. Morin, A. Busch, J. F. Young, S. R. Johnson, J. MacKenzie, and T. Tiedje, Appl. Phys. Lett. **70**, 1438 (1997).
- ¹⁴V. N. Astratov, I. S. Culshaw, R. M. Stevenson, D. M. Whittaker, M. S. Skolnick, T. F. Krauss, and R. M. D. L. Rue, J. Lightwave Technol. **17**, 2050 (1999).
- ¹⁵O. Kilic, S. Kim, W. Suh, Y.-A. Peter, A. S. Sudbø, M. F. Yanik, S. Fan, and O. Solgaard, Opt. Lett. **29**, 2782 (2004).
- ¹⁶V. Lousse, W. Suh, O. Kilic, S. Kim, O. Solgaard, and S. Fan, Opt. Express **12**, 1575 (2004).
- ¹⁷K. B. Crozier, V. Lousse, O. Kilic, S. Kim, S. Fan, and O. Solgaard, Phys. Rev. B **73**, 115126 (2006).
- ¹⁸D. M. Mittleman, *Sensing with Terahertz Radiation* (Springer-Verlag, Heidelberg, 2002).
- ¹⁹Z. Jian, J. Pearce, and D. M. Mittleman, Opt. Lett. **29**, 2067 (2004).
- ²⁰Z. Jian, J. Pearce, and D. M. Mittleman, Semicond. Sci. Technol. **20**, 300 (2005).
- ²¹Z. Jian and D. M. Mittleman, Appl. Phys. Lett. **87**, 191113 (2005).
- ²²Z. Jian and D. M. Mittleman, Phys. Rev. B **73**, 115118 (2006).
- ²³Y. Zhao and D. Grischkowsky, Opt. Lett. **31**, 1534 (2006).
- ²⁴N. Jukam and M. S. Sherwin, Appl. Phys. Lett. **83**, 21 (2003).
- ²⁵D. Grischkowsky, S. Keiding, M. van Exter, and C. Fattinger, J. Opt. Soc. Am. B **7**, 2006 (1990).
- ²⁶P. R. Smith, D. H. Auston, and M. C. Nuss, IEEE J. Quantum Electron. **24**, 255 (1988).
- ²⁷R. Neelamani, H. Choi, and R. Baraniuk, IEEE Trans. Signal Process. **52**, 418 (2004).